Electronic Supplementary Material (ESI) for ChemComm.

This journal is © The Royal Society of Chemistry 2023

ELECTRONIC SUPPLEMENTARY INFORMATION

Alkali carbonate induced N-doping NiSn@NC for direct aqueous ethanol coupling to C_{6+} higher alcohols

Yongjun Ling [a,1], Junwei Liao [a,1], Yuanfei Xie [a], Songbai Qiu [a,b,c], Xiaoping Wu [a,b,c], Qingwei Meng [a,b,c], Qian Zhang [a,b,c,*], Tiejun Wang [a,b,c,*]

a School of Chemical Engineering and Light Industry, Guangdong University of Technology, Guangzhou 510006, China

b Guangdong Provincial Key Laboratory of Plant Resources Biorefinery, Guangzhou 510006, China

c Jieyang Branch of Chemistry and Chemical Engineering Guangdong Laboratory, Jieyang 515200, China.

∗ Corresponding author at: School of Chemical Engineering and Light Industry, Guangdong University of Technology, Guangzhou 510006, China.

E-mail addresses: zhangqian@gdut.edu.cn (Q. Zhang), tjwang@gdut.edu.cn (T. Wang).

[1] These authors contributed equally to this work.

Contents

1. Experimental

1.1 Chemicals

$Ni(NO_3)_2·6H_2O$ (98.0%), $NiCO_3$ (98.0%), $SnCl_4·5H_2O$ (99.9%), $NaHCO_3$（99.0%）, Na_2CO_3 (Na_{CO}, 99.0%), $KHCO_3$（99.0%）, K_2CO_3 (K_{CO}, 99.0%), NaCl（99.0%）, KCl（99.0%）, $NaNO_3$（99.0%）, $C_6H_5Na_3O_7$ (Sodium citrate, Na_{CT}, 99.0%), $C_6H_5K_3O_7$ (Potassium citrate, K_{CT}, 99.0%) and $C_6H_8O_7$ (Citric acid, 99.0%) were purchased from Macklin Biochemicals Ltd. (Shanghai, China) and used without further purification.

1.2 Catalysts synthesis

Preparation of NiSn@NC catalyst:

The N-doped NiSn@C catalysts were fabricated by facile gel-carbonization strategy, typical process is shown in Figure 1a. Typically, the alkali citrate (sodium citrate or potassium citrate) were directly used as the alkali metal inducer for N-doping, and act as metal complexing agent at the same time. First, sodium citrate (Na_{CT}) or Potassium citrate (K_{CT}), $Ni(NO_3)_2·6H_2O$ and $SnCl_4·5H_2O$ were dissolved in deionized water (60 ml) sequentially to obtain a homogeneous solution, the molar ratio is Citrate: Ni: Sn: Alkali metal =4: 1: 0.05: 12. The above solution was then gelled at 80 ^oC with stir and fully dried at 100 ^oC for 48 h. The dried sample was then carbonized under N_2 at 550 ^oC for 2 h with 3 ^oC/min ramp rate. The obtained catalyst was denoted as NiSn@NC-Na_{CT} and NiSn@NC-K_{CT}. To further demonstrate the effect of N doping in NiSn@NC, nonnitrogenous $NiCO_3$ and Ar were also adopted to replace $Ni(NO_3)_2·6H_2O$ and N_2, respectively.

The additional alkali metal salts were also adopted as the N-doping inducer instead of alkali citrates. Here, the cation of alkali metal salt is one of Na^+, K^+, Li^+, and the anion is one of HCO_3^-, CO_3^{2-}, Cl^-, NO_3^-. Typically, citric acid, $Ni(NO_3)_2·6H_2O$, $SnCl_4·5H_2O$ and alkali metal salt were used as the starting material and then fellow the

same gel-carbonization process above-mentioned, the molar ratio is Citrate: Ni: Sn: Alkali metal =4: 1: 0.05: 12. The obtained catalyst was noted as NiSn@NC-x, x is the specific alkali metal salt. For the catalysts fabricated with various Na_2CO_3 content, the molar ratio is Citrate: Ni: Sn: Na_2CO_3 =4: 1: 0.05: (3, 6, 9, 12, 15), the obtained catalysts were noted as NiSn@NC-Na_2CO_3-y, y is the Ni/Na mole ratio of 1/3~1/15.

Preparation of NiSn@C catalysts:

The NiSn@C catalyst without adding alkali metal inducer were prepared for comparison. The $C_6H_8O_7$ (Citric acid), $Ni(NO_3)_2 \cdot 6H_2O$ and $SnCl_4 \cdot 5H_2O$ were used as the starting material and then fellow the same gel-carbonization process with NiSn@NC catalysts. The obtained catalyst was denoted as NiSn@C.

1.3 Catalyst characterization and computational details

N_2 adsorption and desorption were performed using a fully automated surface area and porosity analyzer TriStar II 3020. The surface area and pore characteristic of the catalysts were analyzed by Brunauer-Emmett-Teller (BET) and Barrett-Joyner-Halanda (BJH) methods, respectively. Phase analysis of the catalyst was performed using a Rigaku X-ray diffractometer, MiniFlex 600, with a scan range of 2θ from 5^o to 80^o. Temperature programmed desorption (CO_2-TPD) used MicrotracBEL-BELCAT-B to determine the base properties of the catalyst. The chemical state of each element was determined by X-ray Photoelectron Spectroscopy (XPS) on Thermo Fisher-Escalab 250Xi. Transmission electron microscopy (TEM) measurements were performed on FEI Talos F200S instrument at 200 kV. Raman spectroscopy used HORIBA Jobin Yvon-LabRAM HR Evolution (532 nm) to analysis the carbon materials. Organic elemental analysis (EA) used ELeemetar-Vario EL cube to measure C and N elemental contents. SEM images used cold field emission environmental scanning electron microscope FEI-Quanta 400 FEG. X-ray absorption fine structure (XAFS) analysis of Ni K-edge was acquired on beamline BL14W1 at the Shanghai Synchrotron Radiation Facility (SSRF). EXAFS fitting was applied on Athena and Artemis software. Wavelet transformation (WT) was also adopted by virtue of the

software package developed by Funke and Chukalina using Morlet wavelet with k = 10, σ = 1. The prepared catalysts were washed with deionized water to remove the alkali metal salt prior to testing, unless otherwise noted. The DFT calculations were carried out to calculate the catalytic dehydrogenation process of ethanol molecule over N-doped NiSn@NC catalyst, using density functional theory with the PBE form of generalized gradient approximation functional (GGA). More details can refer to the Supporting Information. The DFT calculations were carried out using density functional theory with the PBE form of generalized gradient approximation functional (GGA) [1]. The Vienna ab-initio simulation package (VASP) [2–5] was employed. The plane wave energy cutoff was set as 400 eV. The Fermi scheme was employed for electron occupancy with an energy smearing of 0.1 eV. The first Brillouin zone was sampled in the Monkhorst-Pack grid [6]. The 3×3×1 k-point mesh for the surface calculation. The energy (converged to 1.0 $\times 10^{-6}$ eV/atom) and force (converged to 0.01eV/Å) were set as the convergence criterion for geometry optimization. The spin polarization was considered in all calculation. The transition state (TS) structures and the reaction pathways were located using the climbing image nudged elastic band (CI-NEB) method [7]. The minimum energy pathway was optimized using the force-based conjugate-gradient method until the maximum force was less than 0.03 eV/Å. The harmonic vibrational frequency calculations were performed to characterize the nature of all the stationary points and to obtain zero point energy (ZPE) corrections. To accurately describe the van der Waals (vdW) interaction, a semiempirical DFT-D3 force-field approach [8,9] is employed in our calculations. For NiSn particle supported on graphene, the NiSn nano-cluster including 36 Ni and 2 Sn atoms was employed to be anchored on the graphene. For pyridine N doped configuration, the defect with pyridine N will be introduced in graphene. In the geometry optimizations, the positions of all the atoms were allowed to relax. A vacuum layer of 18 Å was employed along the c direction to avoid periodic interactions.

1.4 Catalytic experiments

The catalytic coupling of aqueous ethanol took place in a 50 ml stainless steel

autoclave with mechanically stirred (MS-50-316L, Anhui Komi Machinery Technology Co., Ltd, Hefei, China). In a typical experimental procedure, 12.5 g of alcohol(ethanol, n-butanol or n-hexyl alcohol), 12.5 g of H_2O, 0.5 g of catalyst and 0.5 g of NaOH were added to the reactor. The autoclave was then sealed and pressurized with N_2 to 6 MPa for leak checking, and followed by hydrogen gas flushing for 3 times to displace air. Finally, the inner hydrogen atmosphere of 0.1 MPa (ambient pressure) was gained. The reaction ramp-up procedure was carried out from room temperature to 250 ^oC within 60 min and maintained at this temperature for 12 h reaction, the stirring rate was set at 500 rpm. To end the reaction, the reaction temperature was immediately cooled down to ambient temperature with ice-water bath. The reusability of the catalysts was also tested, the catalysts were recovered by filtration, washed with deionized water and ethanol for four times, and dried in vacuum at 60 ^oC for 24 h before directly used for next run.

1.5 Product analysis

The gaseous products were released and collected with gas bag during the decompression process, and the gas volume was determined by drainage method. The gas was analyzed through the FID and TCD detectors of a gas chromatograph (Agilent 8860). The liquid product was collected and weighed, then centrifuged to obtain aqueous and organic phase samples. The liquid phase samples were quantified on a Shimadzu 2010 Pro GC system equipped with HP-INNOWax column (30 m×0.32 mm×0.50 um) based on internal standard method. The n-pentanol was used as the internal standard, the dimethyl sulfoxide (DMSO) and acetone were adopted as the solvent for the aqueous phase and organic phase samples, respectively. Finally, the catalytic performance was evaluated based on ethanol conversion, product yield and selectivity according to Eq. (1-3), respectively.

$$\text{Conversion (X)} = \frac{\text{Moles of } alcohol \text{ disappeared}}{\text{Moles of } alcohol\ before \text{ the reaction}} \times 100\%$$

Eq. (1)

Yield $$(Y) = \frac{\text{Moles of carbon in the product}}{\text{Moles of carbon in ethanol } before \text{ the reaction}} \times 100\%$$ Eq. (2)

Selectivity $$(S) = \frac{\text{Moles of carbon in the target product}}{\text{Moles of carbon in all product}} \times 100\%$$ Eq. (3)

2. Catalyst characterization

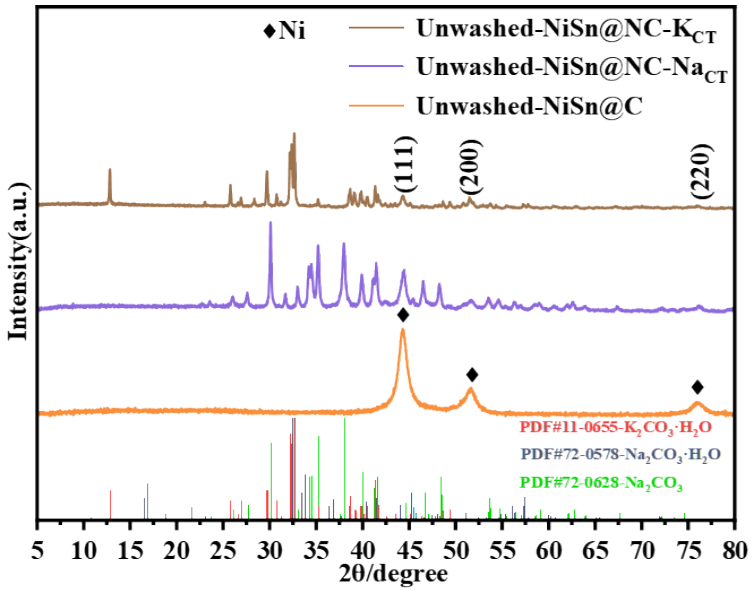

Figure S1. XRD patterns of fresh prepared NiSn@NC-Na$_{CT}$, NiSn@NC-K$_{CT}$ and NiSn@C catalysts.

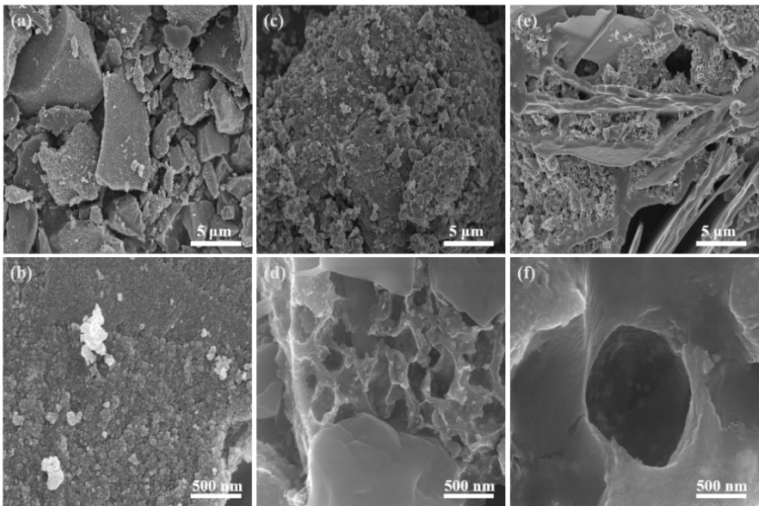

Figure S2. SEM images of (a, b) NiSn@C, (c, d) NiSn@NC-Na_{CT} and (e, f) NiSn@NC-K_{CT}.

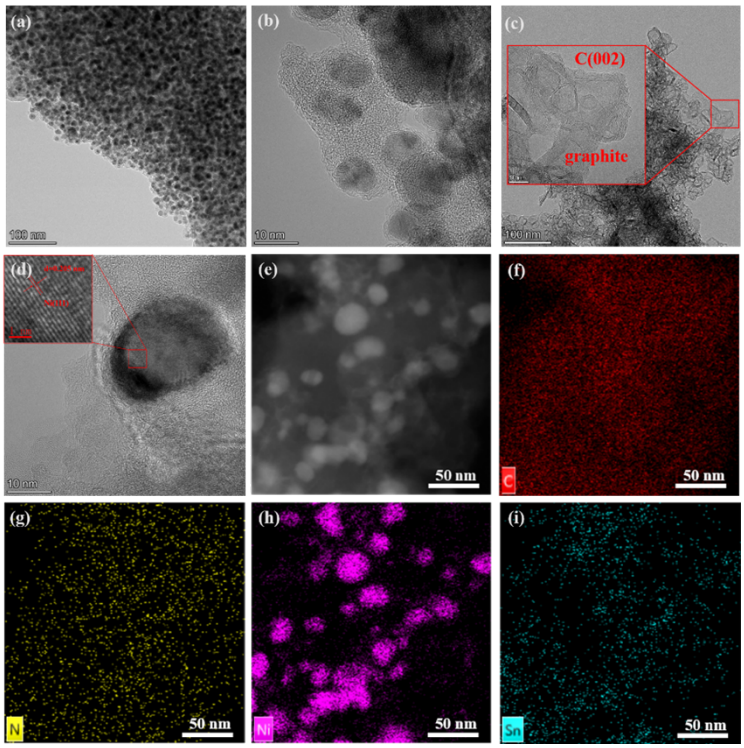

Figure S3. TEM of catalysts prepared using citric acid, sodium citrate, and potassium citrate as carbon sources (a-b) NiSn@C, (c-d) NiSn@NC-K_{CT}, (e) HAADF image of NiSn@NC-Na_{CT} and (f-i) STEM-EDX mapping images of NiSn@NC-Na_{CT}.

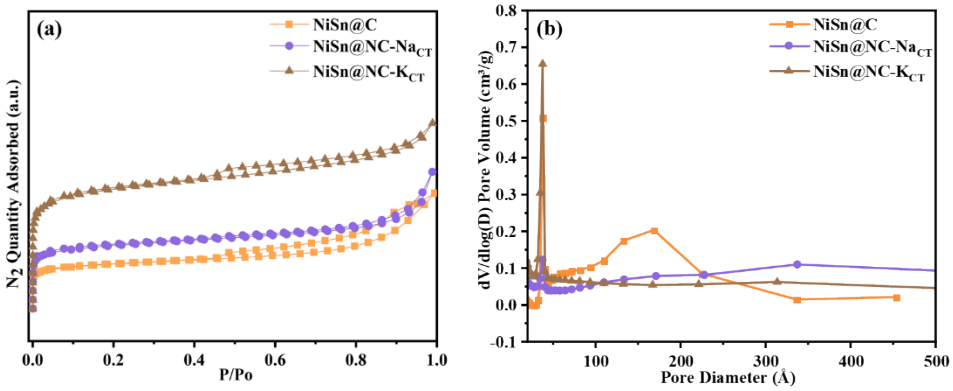

Figure S4. Catalyst prepared with citric acid, sodium citrate and potassium citrate as carbon sources (a) N_2 adsorption/desorption isotherms, (b) pore distributions.

Table S1. Physical properties of the NiSn@C, NiSn@NC-Na_{CT} and NiSn@NC-K_{CT} catalysts.

Catalyst[b]	S_{BET} (m^2/g)	Pore Volume (cm^3/g)[a]	Average Pore D (nm)[a]
NiSn@C	182	0.14	8.69
NiSn@NC-Na_{CT}	245	0.15	9.02
NiSn@NC-K_{CT}	448	0.15	5.52

[a] The pore volume and average pore diameter of catalyst were calculated based on BJH desorption method.

[b] The catalysts were washed to remove the alkali metal salt before characterization.

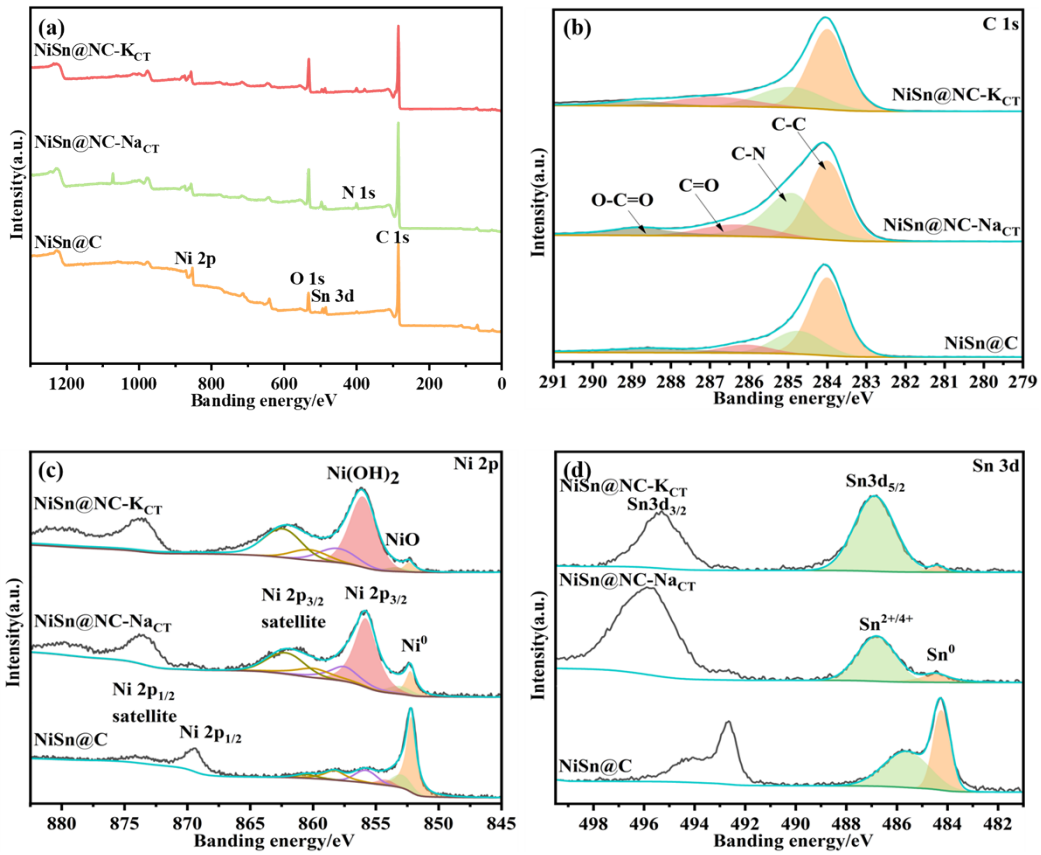

Figure S5. XPS spectra of NiSn@C, NiSn@NC-Na_{CT} and NiSn@NC-K_{CT} catalysts: (a) Survey spectra, (b) C 1 s spectra, (c) Ni 2p spectra, (d) Sn 3d spectra.

Table S2. Contents of N species over different catalysts.

Catalyst	Total N %[a]	Surface N%[b]	N species (%)		
			Pyridinic N	Pyrrolic N	Graphitic N
NiSn@C	0.18	1.6	23.0	60.9	10.8
NiSn@NC-Na_{CT}	2.70	3.5	30.4	47.9	10.9
NiSn@NC-K_{CT}	2.05	3.2	33.2	39.4	14.3

[a] Total N content from elemental analysis (EA) results.

[b] Surface N content from XPS analysis.

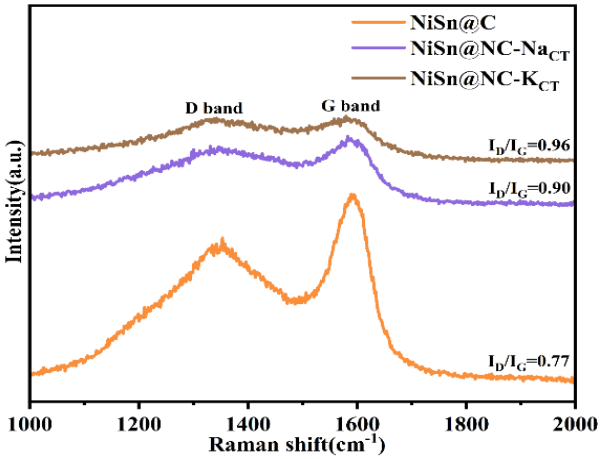

Figure S6. Raman spectra of the NiSn@C, NiSn@NC-Na_{CT} and NiSn@NC-K_{CT} catalysts.

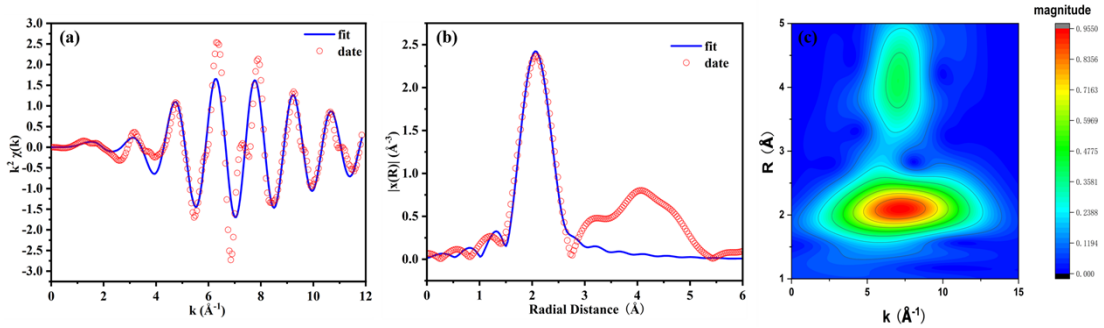

Figure S7. XANES spectra of NiSn@NC-Na_{CT} catalyst: (a) Ni K-edge EXAFS (points) and fit (line) for the NiSn@NC-Na_{CT}, shown in k^2 weighted k-space, (b) Ni K-edge

EXAFS (points) and fit (line), shown in k^2 weighted R-space and (c) Wavelet transform contour plot at Ni K-edge.

Table S3. Fitting parameters for Ni K-edge EXAFS for the NiSn@NC-Na_{CT}.

Paths	CN	R	σ2
Ni-Ni	5.9±0.4	2.48	0.005

S_0^2 was obtained from Ni foil and fixed as 0.90. ΔE_0 was returned a value of -7.1192 ± 0.7085 eV. Data ranges 3.0 ≤ k ≤ 9.9 $Å^{-1}$, 1.5 ≤ R ≤ 2.5 Å. The number of variable parameters is 2, out of a total of 4.2813 independent data points, R factor for this fit is 0.80%. The Debye-Waller factors and delta Rs are obtained based on the guessing parameters and constrained.

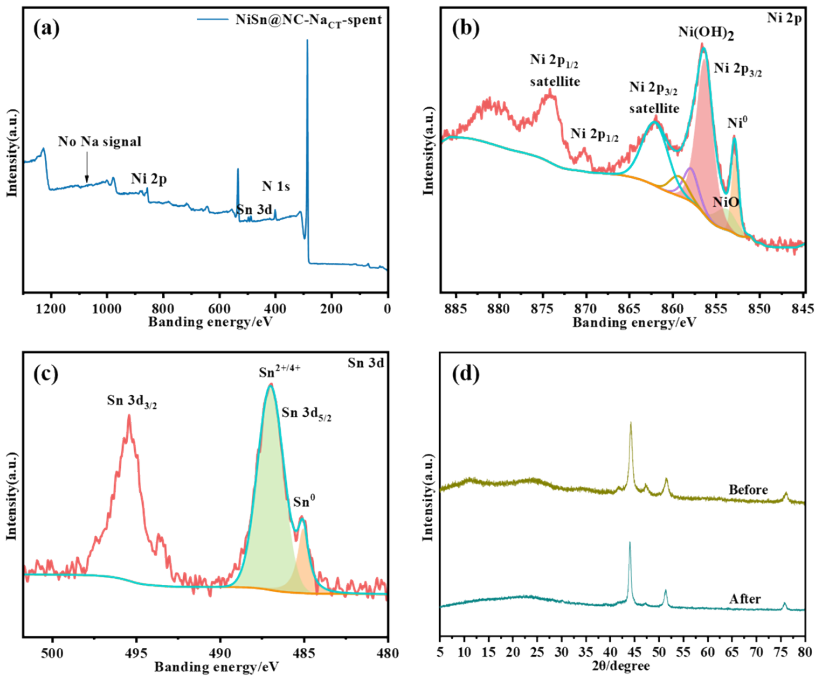

Figure S8. (a-c) XPS spectra of the spent NiSn@NC-Na_{CT} catalyst, (d) XRD of NiSn@NC-Na_{CT} catalyst before and after reaction.

Table S4. Analysis of organic elements in catalysts prepared by pyrolysis of different precursors based on Na_{CT} in N_2 or Ar atmosphere.

Precursors of NiSn@NC-Na_{CT}	Total N (wt%)	C (wt%)
$Ni(NO_3)_2$-N_2	2.70	49.82
$NiCO_3$-N_2	0.22	54.67
$Ni(NO_3)_2$-Ar	2.78	47.89
$NiCO_3$-Ar	--	57.36

Table S5. Elemental analysis of NiSn@NC-Na_2CO_3-y catalysts prepared with different content of Na_2CO_3.

y=Ni/Na	N(wt%)	C (wt%)
1/3	3.29	51.41
1/6	3.62	51.30
1/9	3.53	49.57
1/12	3.51	50.37
1/15	3.26	51.05

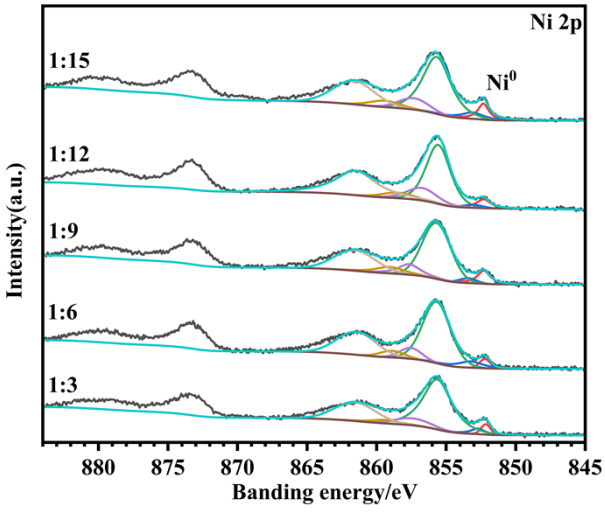

Figure S9. Ni 2p XPS spectra of NiSn@NC-Na_2CO_3-y catalysts(y=Ni/Na ratio=1/3, 1/6, 1/9, 1/12 and 1/15).

3. Experimental data

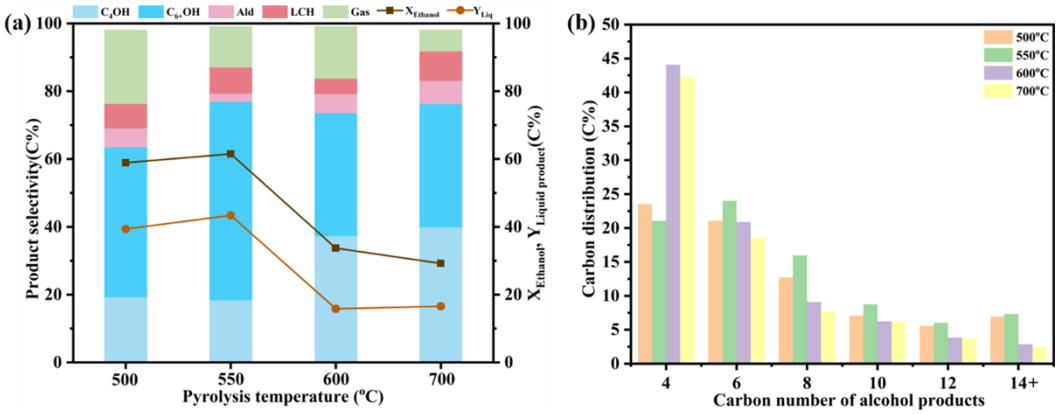

Figure S10. NiSn@NC-Na_{CT} catalysts prepared at different carbonization temperatures (a) ethanol conversion, yield, product selectivity and (b) carbon distribution of liquid product (C_4OH: 1-butanol, $C_{6+}OH$: C_{6+} higher alcohols, Ald: aldehydes, LCH: liquid hydrocarbons, Gas: gaseous carbonous products).

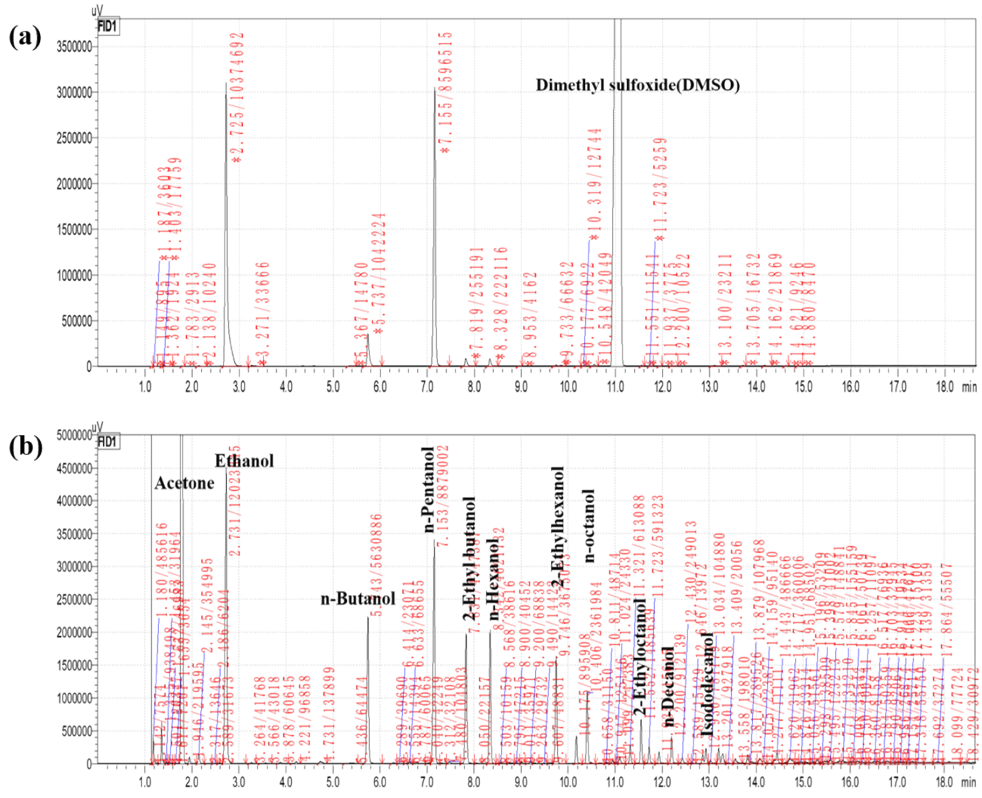

Figure S11. Typical GC results of products obtained from ethanol aqueous coupling

over NiSn@C-Na_{CT} catalyst: (a) Water phase, (b) Oil phase.

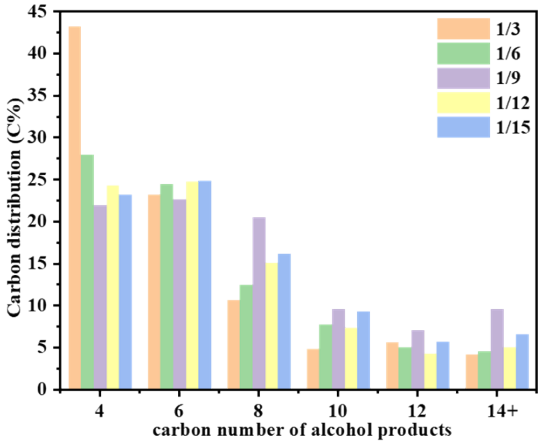

Figure S12. Carbon distribution of alcohol product of NiSn@NC-Na_2CO_3-y catalysts prepared with different Na_2CO_3 content (y=Ni/Na ratio=1/3, 1/6, 1/9, 1/12 and 1/15).

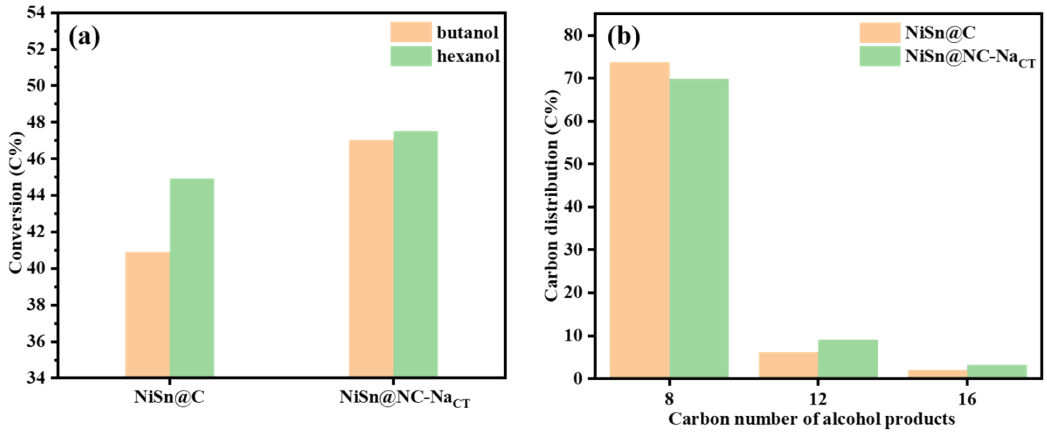

Figure S13. (a) The butanol and hexanol coupling activity over NiSn@C and NiSn@NC-Na_{CT} catalyst, (b) Carbon number distribution of butanol coupling over NiSn@C and NiSn@NC-Na_{CT} catalysts.

4. DFT result

According to the computational details, the initial NiSn nano-cluster/NC and NiSn nano-cluster/C models were constructed by modeling the optimized NiSn nano-cluster on the graphene layer with or without pyridine N defect , respectively (Figure 5b). The

free energy and reaction configurations are shown in Figure 5, it can be seen that the C_2H_5OH adsorption on the top of Ni atom and its dehydrogenation prefer to occur on the bridge sites (Figure 5b-c). The free energy of stable $C_2H_5O^*$ over NiSn nano-cluster/NC is -0.700 eV, which is much lower than 0.078 eV of NiSn nano-cluster/C. This result indicating that the dehydrogenation of C_2H_5OH can be proceeded much more easily over NiSn@NC-Na_{CT} than NiSn@C, which indicates the strong dehydrogenation activity of NiSn@NC-Na_{CT} and this is well in agreement with our experimental results.

Meanwhile, the differential charge diagram indicates that the charge transfer occurred from the NiSn cluster to graphite support. Specifically, the Ni donates more electron to NC (0.89 e) than graphite (0.79 e), which suggesting strong interaction can be found on NC and NiSn cluster. For the dehydrogenation of C_2H_5OH, it's observed that the strong adsorption of C_2H_5OH contribute to low barrier of dehydrogenation. Significantly, the bond orbital analysis of ethanol adsorption indicates that Ni-4s orbital greatly contributed to the adsorption bonding process rather than Ni-3d, which indicated that crucial role of Ni-4s orbital in the adsorption and dehydrogenation of C_2H_5OH. Further partial density of state (PDOS) of Ni-4s proves that the NiSn nano-cluster/NC with elevated Ni-4s band center (-1.39 eV) showed stronger adsorption and lower barrier for C_2H_5OH dehydrogenation than that of NiSn nano-cluster/C (-1.43 eV). On the other hand, the Ni-3d band center for both two systems are the same (-1.11 eV).

5. Reusability of the NiSn@NC-Na_{CT} catalyst

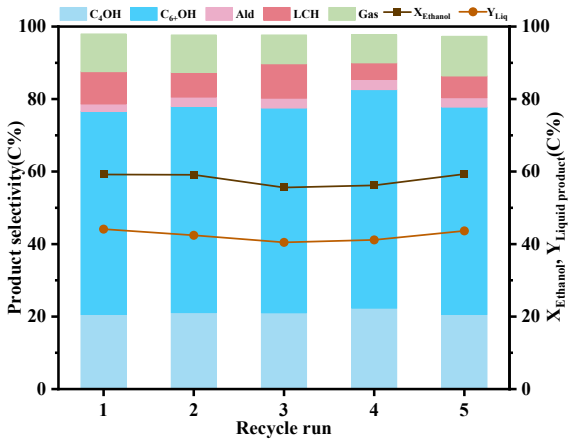

Figure S14. Recycle performance and hydrothermal stability of the NiSn@NC-Na_{CT} catalyst.(The catalyst used for the first time was 0.5012g, the first cycle was 0.475g, the second cycle was 0.456g, the third cycle was 0.430g and the fourth cycle was 0.410g.)

6. Comparison of catalytic properties

Table S6. The performance of ethanol upgrading to high carbon alcohols reported in literatures

Catalyst	Feeding	Reaction condition T (℃)-t (h)	Conversion (C%)	C_4OH Selectivity (C%)	$C_{6+}OH$ Selectivity (C%)	Reference
NiSn@NC-Na_2CO_3-1/9	50% Aqueous ethanol	250-12	57.1	18.8	61.9	This work
MgO	Ethanol	380	7.9	40.0	0.0	[10]
RuNi@MOF	Ethanol	170	11.2	79.0	--	[11]
Metal (Mg, Ca, Sr) phosphates	Ethanol	360	4.2	35.0	0.0	[12]
Ir and Ni_2 tandem	Ethanol	150-24	37.0	>99.0	--	[13]
$Cu_{10}Ni_{10}$-PMO	Ethanol	320	47.9	72.0	--	[14]
Cu_{20}PMO	Ethanol	320	59.0	53	17.0	[15]
Ag-Mg_4Al-LDO	Ethanol	350	44.1	76.2	>8.0	[16]
Mn	Ethanol	160	12.6	79.0	--	[17]
ZrO_2-Y_2O_3	Aqueous ethanol	300	24.7	63.9	>2.3	[18]

* --: No numerical values are given in the references

7. References

1 J. P. Perdew, K. Burke and M. Ernzerhof, *Phys. Rev. Lett.*, 1996, **77**, 3865–3868.

2 G. Kresse and J. Furthmüller, *Computational Materials Science*, 1996, **6**, 15–50.

3 G. Kresse and J. Hafner, *Physical Review B*, 1993, **47**, 558-561.

4 G. Kresse and J. Hafner, *Phys. Rev. B*, 1994, **49**, 14251–14269.

5 G. Kresse and J. Furthmüller, *Phys. Rev. B*, 1996, **54**, 11169–11186.

6 H. J. Monkhorst and J. D. Pack, *Phys. Rev. B*, 1976, **13**, 5188–5192.

7 G. Henkelman, B. P. Uberuaga and H. Jónsson, *The Journal of Chemical Physics*, 2000, **113**, 9901–9904.

8 S. Grimme, *J. Comput. Chem.*, 2006, **27**, 1787–1799.

9 S. Grimme, J. Antony, S. Ehrlich and H. Krieg, *The Journal of Chemical Physics*, 2010, **132**, 154104.

10 S. Hanspal, Z. D. Young, H. Shou and R. J. Davis, *ACS Catal*, 2015, **3**, 1737–1746.

11 C. N. Neumann, S. J. Rozeveld, M. Yu, A. J. Rieth and M. Dinca, *J Am Chem Soc*, 2019, **141**, 17477–17481.

12 S. Hanspal, Z. D. Young, J. T. Prillaman and R. J. Davis, *Journal of Catalysis*, 2017, **352**, 182–190.

13 S. Chakraborty, P. E. Piszel, C. E. Hayes, R. T. Baker and W. D. Jones, *J. Am. Chem. Soc*, 2015, **45**, 14264–14267.

14 Z. Sun, A. Couto Vasconcelos, G. Bottari, M. C. A. Stuart, G. Bonura, C. Cannilla, F. Frusteri and K. Barta, *ACS Sustainable Chem. Eng.*, 2017, **5**, 1738–1746.

15 J. A. Barrett, Z. R. Jones, C. Stickelmaier, N. Schopp and P. C. Ford, *ACS Sustainable Chem. Eng.*, 2018, **6**, 15119–15126.

16 J. Zhang, K. Shi, Y. Zhu, Z. An, W. Wang, X. Ma, X. Shu, H. Song, X. Xiang and J. He, *ChemistryOpen*, 2021, **10**, 1095–1103.

17 S. Fu, Z. Shao, Y. Wang and Q. Liu, *J. Am. Chem. Soc.*, 2017, **139**, 11941–11948.

18 N. V. Vlasenko, P. I. Kyriienko, K. V. Valihura, G. R. Kosmambetova, S. O. Soloviev and P. E. Strizhak, *ACS Omega*, 2019, **4**, 21469–21476.